Journal of Molecular Liquids 277 (2019) 996–1004

Contents lists available at ScienceDirect

Journal of Molecular Liquids

journal homepage: www.elsevier.com/locate/molliq

Aggregate dispersions to enhance the intrachain order in surfactant-stabilized aqueous colloids of poly(3-hexylthiophene)

McKenna Andrews, Anna Smirnova, Devin Sharp, Sarah Taylor, John Cobb, David Boucher *

College of Charleston, Department of Chemistry and Biochemistry, 66 George St., Charleston, SC 29401, USA

ARTICLE INFO

Article history:
Received 25 October 2018
Received in revised form 14 December 2018
Accepted 6 January 2019
Available online 8 January 2019

Keywords:
Poly(3-hexylthiophene)
PCBM
Colloids
Aggregates
Emulsion

ABSTRACT

Aqueous colloids of conjugated polymers (CP), such as poly(3-hexylthiophene) (P3HT), are an attractive alternative for processing CP-based materials because (1) the microstructure of the conjugated polymers can be optimized during the formation of the colloid and (2) this method can significantly reduce the amount of hazardous organic solvents used during manufacturing. This investigation addresses the optimization of the polymer structure by studying the intrachain order of P3HT aggregates pre-assembled in mixtures of chloroform (CF) with dichloromethane (DCM) and subsequently dispersed in aqueous solutions of the surfactant sodium dodecyl sulfate (SDS) using a mini-emulsion method. Compared to an amorphous solution of P3HT, the observed intrachain order of P3HT in the colloids is much higher when using aggregate dispersions pre-assembled in the CF:DCM mixtures. Similar results are observed for aggregate dispersions of a benchmark organic photovoltaic system composed of P3HT and the fullerene derivative phenyl-C_{61}-butyric acid methyl ester (PCBM), but in this case the intrachain order of P3HT in the P3HT:PCBM colloids is anomalously higher than the pure P3HT colloids. Atomic force microscopy (AFM) imaging reveals changes in the dominant structural motifs and morphology of the colloidal P3HT films, but not in a way that correlates with films processed from the aggregate dispersions.

1. Introduction

Poly(3-hexylthiophene) is a benchmark conjugated semiconducting polymer for organic photovoltaic and optoelectronic devices. The interest in P3HT is driven mainly by its intrinsic optical and electronic properties, e.g., wide band-gap and high exciton mobility along the polythiophene backbone, and, their promise for low-cost, large-scale, solution processable manufacturing. However, conjugated polymers like P3HT suffer from lower free charge densities, because of inherent electronic and structural disorder in the functional composites and films generate intrinsic trap sites that create energy loss and charge recombination pathways [1–8]. Several avenues of research have been established to address this problem. Varying the solvent, temperature, deposition methods, and annealing conditions during device fabrication are common techniques used to minimize the structural inhomogeneity of P3HT-based materials [9–11]. Recently, colloids of P3HT have attracted attention as an alternative route for achieving additional control over the morphology and structural order of P3HT films and composites. Directed self-assembly of P3HT into an array of hierarchical nanostructures with disparate molecular packing characteristics can be carried out in the liquid phase during the formation of the colloid. Thus, optimization of the morphology and structural attributes of P3HT can be realized, at least partially, prior to processing and integration of the pre-assembled nanostructures into the functional materials.

Several techniques have been developed to direct the growth of P3HT aggregates and nanostructures in liquid phase colloids [12–21]. Our group primarily focuses on mixed solvent systems to control the assembly of P3HT via the addition of poor or marginal organic solvents to a solution of well-dissolved amorphous P3HT. We have used solubility parameters, solvatochromic parameters, and computational methodologies to investigate the correlation between the composition of the solvent mixtures, the solubility of P3HT in the solvents and solvent mixtures, the structural order of P3HT aggregates in the colloidal dispersions, and the morphological characteristics of P3HT films processed from the dispersions [22–27]. Colloids of P3HT can also be generated using the *mini-emulsion method* [28,29], wherein the organic solvent is removed, e.g., by heating, from a P3HT solution that has been suspended in a solvent that is immiscible with P3HT and the solvent in the solution. The resultant P3HT emulsions are typically stabilized by surfactants, such as sodium dodecylsulfate (SDS) [30–32]. Because P3HT is insoluble in water, the mini-emulsion method is particularly effective for preparing stable aqueous suspensions of P3HT.

Recently, Tan et al. used three different surfactants to demonstrate that the optical properties of aqueous P3HT colloids could be tuned by varying the conjugation length of the surfactant [31]. In that study, all colloids were prepared using solutions of P3HT in chloroform (CF), and the authors reported similar morphology and crystallinity of P3HT

* Corresponding author.
E-mail address: boucherds@cofc.edu (D. Boucher).

https://doi.org/10.1016/j.molliq.2019.01.031
0167-7322/

in the colloids. In a follow-up study, Tan and co-workers used a marginal solvent for P3HT, tetrahydrofuran (THF), to pre-age a P3HT/polystyrene (P3HT/PS) mixture dissolved in chloroform before processing the aqueous P3HT/PS colloids stabilized with sodium dodecylbenzenesulfonate (SDBS) surfactant [30]. Again the authors observed notable changes in the optical properties of the colloids when they used the CF:THF mixtures, as well as increases in the hole mobility field effect transistors (FETs) compared to FETs using colloids made from solutions without THF. So, there is evidence in the literature of both tunabilities of the optical and structural properties of P3HT in aqueous colloids, as well as improved device performance, but these studies are still relatively scarce and the subject is ripe for further scrutiny.

In this paper we discuss the characteristics of aqueous colloids of P3HT and P3HT:PCBM stabilized by the sodium dodecylsulfate (SDS) surfactant. The colloids are processed from aggregate dispersions of P3HT and P3HT:PCBM that we fabricated in several solvent mixtures of chloroform and dichloromethane (DCM) using an interfacial (FAC) growth technique. We recently demonstrated that the FAC method affords a greater level of control over the extent of aggregation and intrachain structural order of P3HT aggregates in CF:DCM mixtures [26]. Thus, it is a suitable technique to study how varying characteristics of the aggregate dispersions impact the attributes of the aqueous colloids. We use UV/Vis absorption spectroscopy, as well as dynamic light scattering and zeta-potential measurements, to investigate the characteristics of the aggregate dispersions and the resulting aqueous colloids. The extent of aggregation and intrachain structural order of P3HT are estimated using the UV/Vis absorption spectra and the methods developed by Spano and co-workers. Additionally, we use atomic force microscopy (AFM) to study the structural motifs and morphology of films processed using the dispersions and colloids. With regard to P3HT:PCBM, this work represents our first application of the FAC technique to this benchmark organic photovoltaic system, and, to our knowledge, this is the first study of aqueous colloids of P3HT:PCBM.

2. Materials and methods

2.1. Materials

Poly(3-hexylthiophene) (P3HT) ($M_n \approx 30$ kDa, regioregularity $\approx 96\%$, PDI < 2) was purchased from Ossila Ltd. and used it without additional purification. Anhydrous solvents (chloroform and dichloromethane), phenyl-C_{61}-butyric acid methyl ester (PCBM), and sodium dodecyl sulfate (SDS) were purchased from Sigma Aldrich and used as received. Ultra-pure, low conductivity water was obtained in-house using a Millipore Milli-Q® Direct 8 water purification system. All anhydrous solvent transfers were performed under an inert environment using air-tight syringes. Prior to preparing the P3HT solutions the anhydrous solvents were filtered through 0.2 μm PTFE filters to remove potential dust and particulates. All glassware used for the P3HT solutions was dried in an oven for >24 h, allowed to cool in a desiccator and then flushed with nitrogen gas to remove dust prior to use.

2.2. Preparation of P3HT dispersions

Aggregate dispersions of P3HT were prepared using two different methods: (1) rapid injection of the poor solvent (DCM) and (2) slow interfacial growth.

2.2.1. Rapid injection of the poor solvent

A stock solution of 5 mg/mL P3HT ($M_n \approx 49.5$ kDa) in chloroform was prepared and stirred at 60 °C for ~3 h until bright orange to ensure complete dissolution of the P3HT. The stock solution was used to prepare 1 mg/mL working solutions of P3HT in mixtures of chloroform (CF) with the poor solvent, DCM. To prepare each 4 mL solution, 0.8 mL aliquot of the 5 mg·mL^{-1} P3HT stock was transferred to a 20 mL scintillation vials (diameter, $D \approx 27$ mm) containing the additional chloroform required to give the desired volume fraction of chloroform in each solution. The volume of DCM needed to give the required volume fraction of the poor solvent was then rapidly injected into the P3HT/CF solutions. The vials were sealed and left to age in the dark and under an atmosphere of dry nitrogen for approximately ~24 h.

2.2.2. Interfacial growth method

A 0.8 mL aliquot of the 5 mg·mL^{-1} P3HT ($M_n \approx 30$ kDa) stock was transferred to a scintillation vial containing the additional chloroform required to give the desired volume fraction of chloroform in each solutions. As shown in Fig. 1(a), a syringe pump was used to add the desired volume of DCM to each P3HT/CF solution. By setting the end of the needle against the side of the vial and letting the poor solvent slowly run down the side of the vial, the DCM formed a separate layer on top of the P3HT/CF solution, as shown in Fig. 1(b). Two vials were used with nominal diameters of $D = 18.75$ mm and $D \approx 27.0$ mm, which correspond to interfacial areas of $A_{int} \approx 2.75$ cm^2 and $A_{int} \approx 5.75$ cm^2, respectively. The vials were sealed and left to age in the dark and under an atmosphere of dry nitrogen for approximately ~24 h, and, as shown in Fig. 1(c), an aggregate dispersion of P3HT is produced as a result of the mixing of the layers.

2.3. Preparation of P3HT:PCBM dispersions

A 50:50 wt%:wt% stock solution of P3HT ($M_n \approx 30$ kDa) and PCBM in chloroform (5 mg/mL) was prepared and stirred at 60 °C for ~5 h until bright orange to ensure complete dissolution of the P3HT. P3HT:PCBM dispersions in CF:DCM solvent mixtures were prepared using the rapid injection and interfacial growth methods, as described above.

2.4. Preparation of P3HT and P3HT:PCBM colloids: mini-emulsion method

A 0.8 mL aliquot of the aged P3HT, or P3HT:PCBM, dispersions was added to 3.2 mL of a 10 mM aqueous solution of SDS (critical micelle concentration, CMC ≈ 8 mM) in a 20 mL scintillation vial. Each solution was sonicated for 5 min and then heated at 70 °C with stirring (~500 rpm) to remove the CF and DCM. Photographs showing the mini-emulsion method are shown in Fig. 2.

2.5. UV/Vis absorption spectroscopy

The aged 1 mg/mL dispersions of pristine P3HT and P3HT:PCBM were diluted by a factor of five in the corresponding solvent mixture. Dilution was necessary to keep the absorbance maximum below one. Following dilution the dispersion was quickly transferred to a 1 mm path length cuvette and the absorption spectra was measured in the 800 nm to 350 nm range with a double beam spectrophotometer (Perkin-Elmer, Lambda 45) using a 0.2 nm step size and 480 nm·min^{-1} scan speed. Absorption spectra of the aqueous P3HT and P3HT:PCBM colloids were measured in a 1 cm path length cuvette. For each solution a reference of the pure solvent was used to baseline the spectrometer prior to acquiring the spectrum.

2.6. Dynamic light scattering

Dynamic light scattering (DLS) measurements were performed on aggregate dispersions and aqueous colloids at the same concentrations as UV/Vis absorption spectra. Glass cuvettes for the DLS measurements were cleaned using a high flow of nitrogen gas to remove large dust and particulates. DLS measurements were performed at 25 °C using a Malvern Zetasizer, Nano ZS instrument equipped with a 633 nm HeNe laser and a narrow bandpass filter centered at 633 nm (10 nm bandwidth) to minimize background fluorescence. Each measurement was corrected using the refractive index and viscosity of the solvent blend, which were measured at 25 °C with an Abbé refractometer and calibrated Cannon-Fenske viscometer. The particle size distribution (PSD)

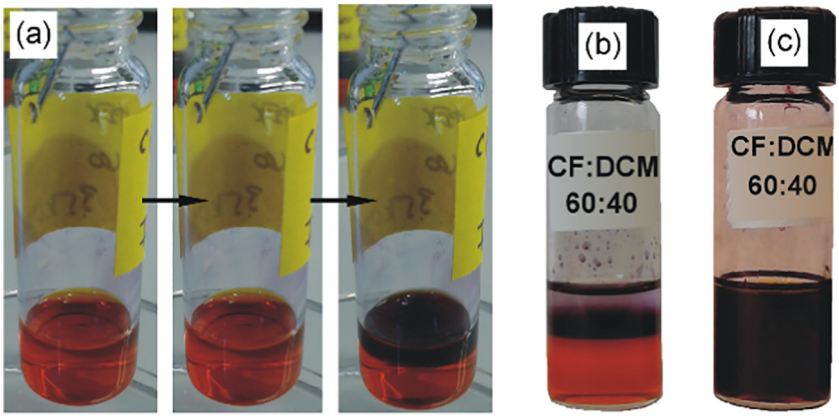

Fig. 1. (a) During the interfacial growth method a syringe pump is used to careful add a layer of the poor solvent, e.g., dichloromethane, on top of a P3HT, or P3HT:PCBM, solution in chloroform. (b) A representative 60:40 CF:DCM sample immediately after adding the top layer of DCM. (c) The same sample in (b) after aging and allowing the layers to mix for ~24 h.

was obtained from the Malvern software and a cumulant analysis within a spherical particle approximation.

2.7. Laser Doppler electrophoresis and zeta potential measurements

For laser Doppler electrophoresis a commercial dip cell (Malvern, ZEN1002) was inserted into the same samples used for the DLS measurements. Each measurement was corrected using the refractive index, viscosity, and dielectric constant of the solvent blend. We approximated the dielectric constant, ε_{mix}, of the solvent mixtures under the assumption that ε_{mix} is linearly additive in terms of the mole fraction composition and dielectric constant of the pure solvents, $\varepsilon_{mix} = X_1\varepsilon_1 + X_2\varepsilon_2$ [33]. For each sample we measured the electrophoretic mobility by varying the applied voltage in 5 V increments in the range 5 V to 100 V until reproducible results were obtained with settings that yielded high quality count rates, distribution data, and phase data.

2.8. Atomic force microscopy (AFM) imaging

P3HT films were processed by spin coating (1000 rpm) 15 μL of the aggregate dispersions onto Piranha cleaned silicon substrates (Ted Pella). Colloid films were prepared by drop casting 15 μL onto Piranha cleaned glass substrates and allowing them to dry overnight in a dessicator. The micro- and nanoscale features of the films were probed under ambient conditions with an atomic force microscope (TT-AFM, AFM Workshop) operating in non-contact mode and using silicon probes (AppNano) with a resonant frequency of 185 kHz ($k \approx 40\ N \cdot m^{-1}$). All scans were conducted using 1024 scan lines and a 0.1 Hz scanning rate. We manually adjusted the PID parameters and the gains of the X-, Y-, and Z piezos to maximize the image contrast and minimize the noise in the *Z*-drive.

Measurements on a pristine silicon substrate revealed that the noise floor of the scanner stage is ~0.1 nm when the Z high-voltage gain is 3 V. We calibrated the AFM using a standard step height reference (AppNano) and processed all phase and amplitude images e.g., leveling and flattening, using Gwyddion software.

3. Results and discussion

3.1. Pure P3HT dispersions and colloids

The results for the aggregate dispersions and aqueous colloids of pure P3HT are shown in Fig. 2. Details for the methods used to calculate R_{abs} and the extent of aggregation (κ) are presented in Section SI in the *Supporting information*. Although the aggregate dispersions generated using binary CF:DCM mixtures are themselves colloids, in this paper we will use the term *dispersion* when referring to these systems. We reserve the term *colloid* when referring to the aqueous SDS-stabilized colloids processed using the min-emulsion method.

The spectra in Fig. 3(a) and R_{abs} and κ values in Fig. 3(b) are in agreement with our previous work. Specifically, we observe a monotonic increase in κ with increasing volume of the poor solvent (DCM) and a maximum R_{abs} value in 60:40 CF:DCM. Additionally, as shown in Table S1 (*Supporting information*), a larger red-shift in the wavelength of the A_1 and A_2 vibronic bands is observed with increasing R_{abs} values. Similarly, as shown in Table S1, there is an attendant decrease in the energy separation of the vibronic peaks, $\Delta E_{vib} = E_{A2}–E_{A1}$, with increasing R_{abs}, which is attributed to the softening of the phonon modes due to the increasing conjugation lengths of the polymer backbone and larger effective delocalization of the π-electrons [34,35]. Thus, the observed trends in R_{abs}, the wavelength of the vibronic bands, and ΔE_{vib} are consistent with higher intrachain order in the P3HT aggregates [24]. The aqueous colloidal dispersions in Fig. 3(c)–(d) exhibit a R_{abs} trend similar to that of the aggregate dispersions in Fig. 3(b). Thus, in general, the intrachain characteristics of the dispersions are transferred to the aqueous dispersions.

We used dynamic light scattering (DLS) to further study the impact of the solvent mixture on the particle size distribution (PSD) of the dispersions and colloids, which are shown in Fig. 4(a) and (b), respectively. Additional details of the DLS data, including graphs of the size corrected (fractional) scattering intensity, $I_{corr} = I_{scatt}/D_H$, are included Section SII in the *Supporting information*. The PSD of amorphous P3HT in pure CF is unimodal with a hydrodynamic diameter $D_H \approx 18$ nm. The size

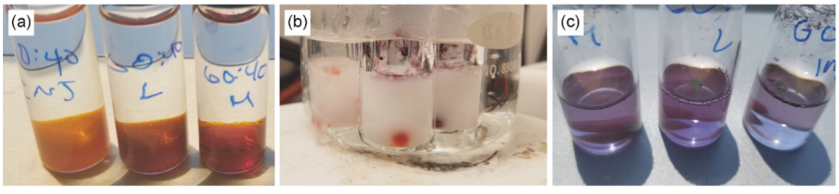

Fig. 2. Representative photographs of the mini-emulsion method. (a) An aliquot of the aggregate dispersion is transferred to 10 mM aqueous SDS solution. (b) The samples in (a) are heated in a 70 °C water bath to remove the CF and DCM. (c) Stable SDS-stabilized colloids are formed after removal of the organic solvents.

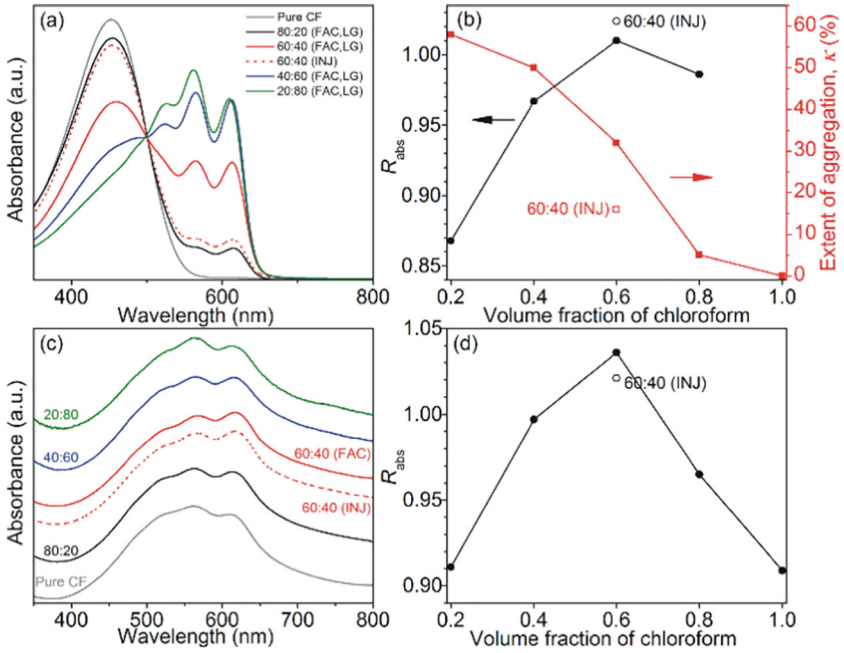

Fig. 3. (a) UV/Vis absorption spectra and (b) the extent of aggregation (red squares) and R_{abs} values (black circles) of aggregate dispersions of P3HT in CF:DCM solvent mixtures. The open symbols in (b) correspond to R_{abs} and κ in the 60:40 CF:DCM INJ dispersion. (c) UV/Vis spectra of the aqueous P3HT colloids prepared using the aggregate dispersions in (a). The spectra have been vertically offset for clarity. (d) R_{abs} values for the colloid spectra in (c), where the open symbol corresponds to the colloid prepared using the 60:40 CF:DCM INJ dispersion.

distribution of the aggregate dispersions are all bimodal, wherein the band at lower D_H is ascribed to residual amorphous P3HT, as well as smaller dimers, trimers, etc., and the band at higher D_H corresponds to larger aggregates. As the amount of DCM increases the smaller D_H band monotonically shifts from ~18 nm in 80:20 CF:DCM to ~56 nm in 20:80 CF:DCM (see Table S4 in the *Supporting information*). Similarly, the band corresponding to the larger aggregates shifts slightly from ~250 nm in 80:20 CF:DCM to ~370 nm in 20:80 CF:DCM, wherein the fractional scattering intensity of these bands (Fig. S4) increases relative to the band at lower D_H. Thus, the trends in the size distributions are consistent with an increase in the extent of aggregation and growth of larger P3HT aggregates with increasing composition of DCM.

The behavior of the PSDs of the aqueous colloids in Fig. 4(b) is notably different than the dispersions in Fig. 4(a). Although bimodal size distributions are observed for the 80:20 and 60:40 CF:DCM systems, the 40:60 and 20:80 CF:DCM dispersions have unimodal PSDs, which slightly shift to smaller D_H with increasing volume fraction of DCM in the solvent mixture used to induce aggregation. Variations in the composition of CF and DCM in the mixtures are expected to affect the formation of the aqueous colloids. The DLS PSDs suggest that the rapid initial evaporation of larger amount of DCM, which leaves a smaller amount of residual CF, tends to collapse the larger surfactant-stabilized P3HT colloids. The unimodal nature of the 40:60 and 20:80 CF:DCM PSDs in Fig. 4(b) also coincide with the aggregate dispersions with larger aggregate phases, κ ≥ 50%. Thus, although the intrachain order of the aggregates is effectively transferred to the P3HT colloids, other characteristics of the dispersions, e.g., solvent composition and extent of aggregation, may significantly affect the properties of the colloids. Indeed, due to the low boiling point of DCM, we observed that the time required for formation of the colloids in the 70 °C bath decreases with increasing DCM composition in the solvent mixture. Although the details of the underlying mechanisms are not known at this time, it is reasonable that the composition of the solvent mixtures influences the kinetics and thermodynamics of the formation of the colloid.

We calculated correlation coefficients (Table S3, *Supporting information*) to further investigate the correspondence between the properties of the dispersions, e.g., R_{abs}, κ, and solvent composition, and the colloids. In the *aggregate dispersions* there are good correlations between R_{abs} and the extent of aggregation, κ, and volume fraction of CF, φ_{CF}, with correlation coefficients $\chi_{R\text{-}\kappa} = -0.70$ and $\chi_{R\text{-}\varphi} = 0.8$, as well as a strong correlation between κ and φ_{CF}, $\chi_{\kappa\text{-}\varphi} = -0.94$. Thus, the extent of aggregation increases with decreasing (increasing) composition of CF (DCM), and, in turn, the intrachain order increases with decreasing κ and increasing φ_{CF}. We have discussed these trends in detail elsewhere

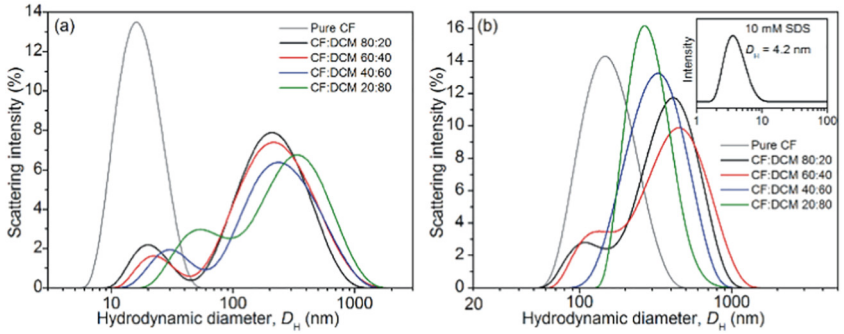

Fig. 4. DLS particle size distributions (PSDs) of (a) pure P3HT aggregates dispersions in CF:DCM solvent mixtures and (b) aqueous P3HT/SDS colloids. The inset in (b) shows the PSD of a 10 mM SDS solution.

[24,25]. Briefly, smaller κ values, which are associated with a higher φ_{CF}, correspond to aggregation of the longer and/or more regioregular P3HT chains, which are capable of achieving longer conjugation lengths, i.e., higher intrachain order, during planarization and π-stacking. In the *aqueous colloids* the correlation coefficient for R_{abs} is largest between R_{abs} in the dispersion, $\chi_{R\text{-}R} = 0.93$, followed by φ_{CF}, $\chi_{R\text{-}\varphi} = 0.5$, and, finally, κ, $\chi_{R\text{-}\kappa} = -0.38$. Therefore, in terms of the correlation coefficients, the R_{abs} values in the aggregate dispersions appear to be the dominant determinant of the intrachain order in the colloids and the extent of aggregation and solvent composition play auxiliary roles.

Despite the strong correlation between R_{abs} in the aggregate dispersions and the colloids, we contend that changes in the solvent composition associated with the evaporation rates and evaporation rate differences of the organic solvents is actually critical to the assembly and molecular order in the colloid during the mini-emulsion process. We make this assertion based on the intrachain order in the 60:40 INJ and 80:20 CF:DCM colloids. The 60:40 CF:DCM INJ and FAC dispersions have comparable intrachain order ($R_{abs,\ FAC} \approx 1.010$ and $R_{abs,\ INJ} \approx 1.021$), but exhibit very different aggregation behavior ($\kappa_{FAC} \approx 32\%$ and $\kappa_{INJ} \approx 16\%$). However, as shown in Fig. 3(d), R_{abs} in the 60:40 CF:DCM FAC colloid is only slightly larger ($R_{abs,\ FAC} = 1.036$) than in the INJ colloid ($R_{abs,\ INJ} = 1.024$). The similarity in R_{abs} is quite striking in light of the difference in κ. As illustrated in Fig. 5(b), if the ~84% P3HT that constitutes the residual amorphous phase in the 60:40 CF:DCM INJ dispersion behaves exactly like the amorphous P3HT/CF solution in Fig. 5(a), we would actually expect R_{abs} in the resultant 60:40 CF:DCM INJ colloid to be significantly lower than it is. The same should also apply to the 80:20 CF:DCM, wherein ~95% exists as amorphous P3HT in the dispersion. The R_{abs} value of the P3HT/CF colloid, Fig. 5(a), is so low ($R_{abs} = 0.909$) compared to the other systems that without a significant solvent effect on the assembly of the colloid it is doubtful that the small aggregate phase in the 80:20 and 60:40 INJ dispersions could offset the large amorphous phase to increase the effective R_{abs} values in the colloids.

Additional evidence of the importance of the organic solvent mixtures is Tan et al. reported changes in the intrachain order of P3HT using CF:THF mixtures, but in that study the R_{abs} values are much lower, $R_{abs} \leq 0.87$, than those reported here [30]. This difference may be partially attributed to the use of THF instead of DCM, where we have shown previously that DCM is a particularly effective solvent for fabricating aggregates with high intrachain order. However, Tan and *co*-workers (1) added polystyrene (PS) to the dispersions and colloids and (2) did not report the UV/Vis absorption spectra or R_{abs} values observed in the P3HT:PS dispersions in CF:THF prior to making the aqueous colloids, both of which preclude a direct comparison of the solvent effects to those observed herein. Additional work focusing on the development of the colloids throughout the mini-emulsion process and using aggregate dispersions in different solvent mixtures is needed to scrutinize the role of the organic solvent in more detail.

3.2. P3HT:PCBM dispersions and colloids

Fig. 6 shows the results for the dispersions and colloids of the P3HT:PCBM systems. Comparisons of the R_{abs} values P3HT and P3HT:PCBM dispersions and colloids are shown in Fig. 7(a) and (b), respectively. Fig. 6(a)–(b) reveal that the trends in κ and R_{abs} are similar to the P3HT dispersions in Fig. 3(a)–(b). The extent of aggregation in the P3HT:PCBM dispersions is comparable to those of pure P3HT, which suggests similar aggregation behavior of P3HT, i.e., similar solvent-P3HT interactions and thermodynamics. Also, like the pure P3HT systems, the R_{abs} values are larger in the aqueous colloids compared to the aggregate dispersions. However, as shown in Fig. 7(a) the intrachain order in the P3HT:PCBM dispersions is notably higher in the 80:20 and 60:40 CF:DCM mixtures relative to pure P3HT, and in Fig. 7(b) R_{abs} for all P3HT:PCBM colloids are larger than the corresponding P3HT colloids. In fact, the $R_{abs} > 1$ for all P3HT:PCBM colloids, thereby indicating highly ordered *J*-type P3HT aggregates in all the colloids. Thus, the presence of the PCBM in the solution does affect the assembly behavior of P3HT at CF:DCM solvent interface, particularly for the 80:20 and 60:40 CF:DCM mixtures.

To corroborate these results we studied the behavior of a different P3HT sample, having a higher molecular mass ($M_n \approx 75$ kDa) but a similar regioregularity ($rr \approx \%$). The results are summarized in Fig. S5 in the *Supporting information*. Despite some minor variations in the assembly behavior the 75 kDa P3HT sample, which may be attributable to the higher molecular mass, we again observe the largest R_{abs} in the colloid processed using the 60:40 CF:DCM mixture. More importantly, as shown in Fig. S5(f), the intrachain order is markedly higher in all the P3HT:PCBM colloids compared to the dispersions, which is similar to the behavior of the 30 kDa P3HT sample.

In an earlier study we showed that the kinetics of mixing of the solvents at the interface varies with the composition of the solvent, which, in turn, affects the properties of the aggregate dispersion, i.e., R_{abs} and κ [26]. As the amount of DCM increases, the mixing time of the CF and DCM layers decreases, which in turn mitigates the interfacial effects. This observation may partially explain the similar characteristics of the 40:60 and 20:80 dispersions of P3HT and P3HT:PCBM in Fig. 7(a). In the 80:20 and 60:40 CF:DCM mixtures the slower rate of mixing may facilitate controlled growth of the P3HT aggregates that is more readily influenced by the presence of PCBM, e.g., akin to a co-crystallization process, and yields aggregates with higher intrachain order. However, at this time it is not clear how the properties P3HT:PCBM dispersions give rise to the significantly larger R_{abs} values in the P3HT:PCBM colloids.

Despite the perceived advantages of surfactant-stabilized P3HT colloids discussed earlier, devices fabricated using materials processed with the mini-emulsion tends to exhibit lower the hole mobility compared those processed from solutions of pristine P3HT [30,31]. The decrease in conductivity in these materials is ascribed to charge trapping mechanisms stemming from insulating effects of the surfactant [30]. Furthermore, it is well-established that the nanostructure and morphology of P3HT films and composites impact the performance of devices, such as solar cells (SCs) and field effect transistors (FETs) [36–42], and additional processes associated with the formation and assembly of the colloids t further complicate optimization of colloidal P3HT materials. However, recently Tan et al. reported an increase in current capacity and hole mobility in FETs processed from surfactant-stabilized P3HT colloids, which was attributed primarily to the increasing conjugation length, *l*, of the three surfactants–(1) SDS, (2) sodium dodecylbenzenesul-fonate (SDBS) and (3) disodium 4-dodecyl-2,4′-

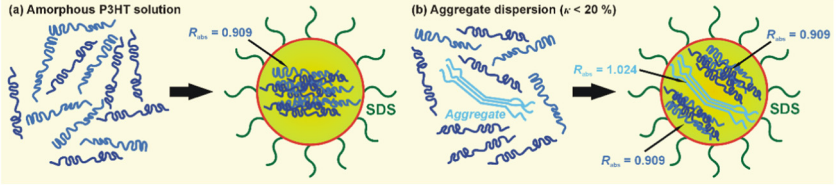

Fig. 5. Cartoons illustrating intrachain order in SDS-stabilized aqueous colloids processed using (a) an amorphous P3HT solutions, and (b) an aggregates dispersion with a moderate extent of aggregation (<20%), wherein the organic solvent mixture does not affect the assembly of the colloid.

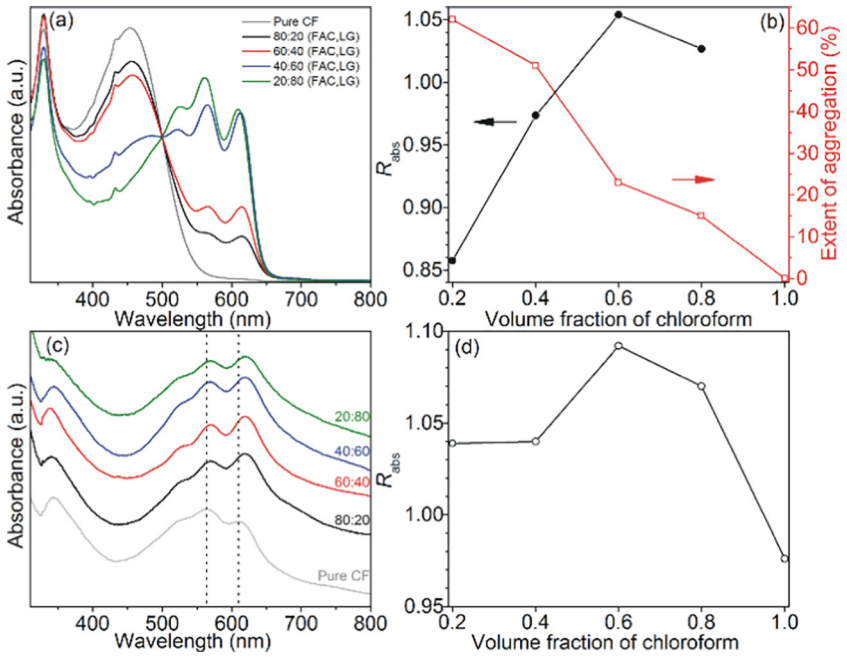

Fig. 6. (a) UV/Vis absorption spectra and (b) the extent of aggregation (red squares) and R_{abs} values (black circles) of aggregate dispersions of P3HT and PCBM in CF:DCM solvent mixtures. (c) UV/Vis spectra of the aqueous P3HT:PCBM colloids prepared using the aggregate dispersions in (a). The spectra have been vertically offset for clarity. (d) R_{abs} values for the colloid spectra in (c).

oxydibenzenesulfonate (DOBS)– used to stabilize the colloid ($l_{SDS} < l_{SBDS} < l_{DOBS}$) [31]. In that study the improved performance of the FETs also correlated with an increase in the R_{abs} values (A_1:A_2 ratio) of P3HT in the colloids and films: R_{abs}(SDS) < R_{abs}(SBDS) < R_{abs}(DOBS) (see Table 1 in ref. 31), thereby indicating that surfactant conjugation increases the intrachain order of P3HT. In the present study we observe a notable increase in the intrachain order of P3HT in the colloids using only one surfactant (SDS). Also, our R_{abs}, values are notably higher than any of those reported by Tan et al. Thus, using solvent mixtures we can obtain significant changes in the intrachain order of P3HT independent of the surfactant, and it will be interesting to observe how our approach is affected by other surfactants, e.g., SBDS and DOBS. If our approach can be successfully extended to much more concentrated P3HT dispersions and colloids, then it will present a unique venue to further study the effect that the intrachain order of P3HT in the colloids has on the performance of the FETs.

3.3. Atomic force microscopy (AFM) imaging: aggregate and colloid films

Fig. 8 shows exemplary AFM height images of pure P3HT films spun cast from pure a CF solution and aggregate dispersions in 80:20, 60:40, 40:60, and 20:80 CF:DCM mixtures. The corresponding phase images are shown in Fig. S7 (*Supporting information*). Fig. 8(a) shows that the amorphous P3HT/CF solution produces a film comprised of small spherical structures. These small spheroidal structures are also prevalent in 80:20 CF:DCM film in Fig. 8(b), but we also observe very thin fibers. In Fig. 8(c), the 60:40 CF:DCM dispersion yields a film composed of dense network of long, high aspect ratio fibers. The 40:60 CF:DCM film in Fig. 8(d) contains a mixture of spheres and fibers, and the 20:80 CF:DCM film in Fig. 8(e) is composed of spheroidal motifs. A complete interpretation of the varying structural motifs and morphologies of the films in terms of solvent evaporation rates, thermocapillary forces, convective assembly, mass transport and surface tension gradients, i.e., Marangoni instabilities, etc., is beyond the scope of this paper. We have discussed some of these factors in more detail in a previous publication [23]. The primary purpose of the AFM images in Fig. 8, is to provide a benchmark to compare the films processed using the aqueous colloids. We do note that the fibrous nature of the film morphology does correlate with the increase in the zeta potential (ζ) of the aggregate dispersions (see Section SIV in the *Supporting Information*), but at this time we are hesitant to suggest a definitive causational relationship between ζ and the dominant structural motifs of the films.

We dried the drop cast P3HT colloid films under a vacuum, which drastically changes the evaporative patterns and macroscopic features

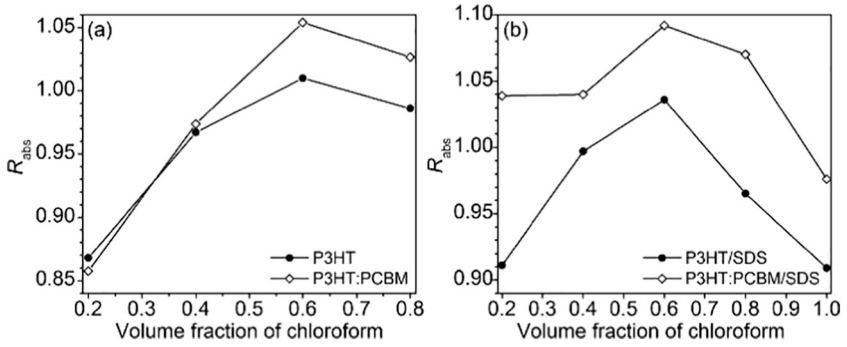

Fig. 7. Comparison of R_{abs} of (a) aggregate dispersions of P3HT (•) and P3HT:PCBM (◦) in CF:DCM solvent mixtures, and (b) the corresponding aqueous colloids of P3HT and P3HT:PCBM prepared using the dispersions in (a).

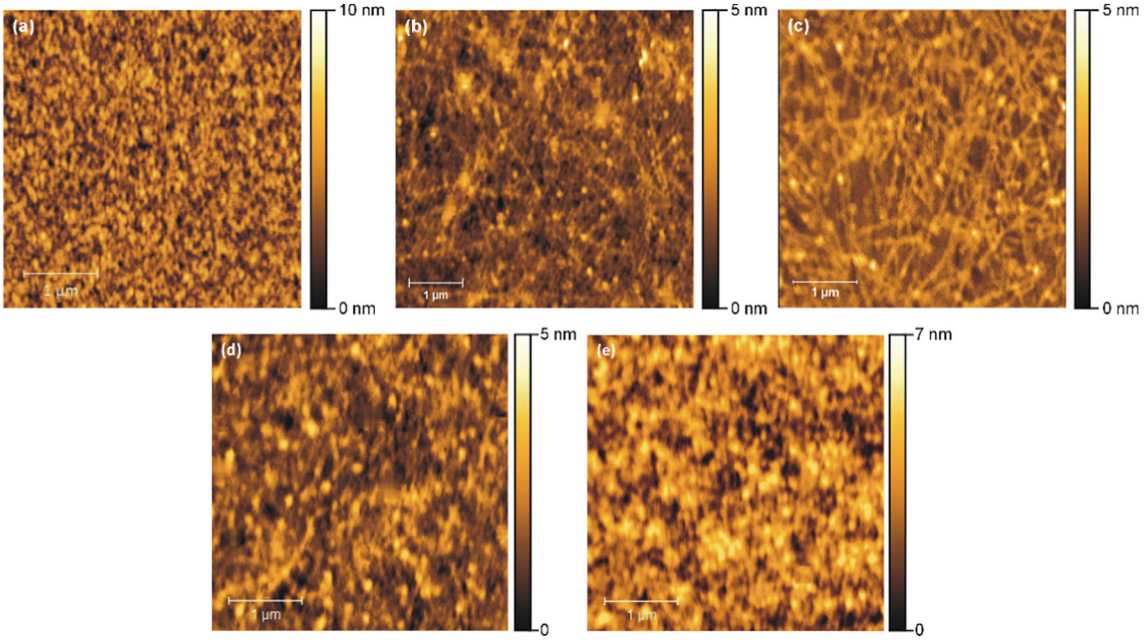

Fig. 8. Tapping mode AFM (TT-AFM) height images of P3HT films ($M_n \approx 30$ kDa) spun cast at 1000 rpm from (a) a 1 mg·mL^{-1} solution in pure CF, and 1 mg·mL^{-1} aggregate dispersions in (b) 80:20, (c) 60:40, (d) 40:60, and (e) 20:80 CF:DCM mixtures.

of the films compared to films dried under ambient conditions. For brevity this topic is discussed in more detail in Section SV in the *Supporting information*. We chose to dry the films under a vacuum because drop casting tends to yield thick and dense films, which makes it difficult to resolve the smaller elemental structural motifs. Conversely, spin-coating the colloids yields a sparse distribution of discrete particles on the substrate. The vacuum drying technique provides a compromise between the two methods, wherein the particle lean regions in the center of the films affords improved surface coverage compared to the spin coated films.

We used atomic force microscopy (AFM) to study the smaller features of the films in the thinner regions proximal to the thick features at the outer edge of the films. The approximate location of the AFM image in each film is denoted by the arrow in the photographs in Fig. S10. (*Supporting information*). The pure SDS film did not reveal remarkable features in the central part of the film, but, as shown in the AFM images in Fig. 9, structural and morphological variations are observed in films processed from the aqueous P3HT colloids. Phase images are shown in Fig. S8 (*Supporting information*).

The 80:20 CF:DCM film in Fig. 9(a) is composed of spheroidal structures. The average diameter of the spheres, $D_{avg} \approx 250 \pm 50$ nm, are similar those observed in films using a colloid processed from a solution of P3HT in chloroform, thereby supporting the supposition that the properties of the 80:20 CF:DCM colloid, i.e., higher volume fraction of CF and low extent of aggregation, are comparable to colloids prepared using an amorphous P3HT solution. As the volume fraction of DCM increases, the spheres in the 60:40 CF:DCM colloid film in Fig. 9 (b) become slightly larger, $D_{avg} \approx 350 \pm 100$ nm. The 40:60 CF:DCM film in Fig. 9(c) is also composed of relatively large particles, $D_{avg} \approx 400 \pm 150$ nm, but, as shown in the inset, they are more ellipsoidal than spherical. The 40:60 CF:DCM film also reveals a notable change in morphology. The ellipsoidal motifs adopt a linear arrangement giving the film a fibrous appearance. The variation of the film morphology is even more apparent in the 20:80 CF:DCM film in Fig. 9(d). Spheroidal features are barely visible and the film consists of a dense fibrilar network reminiscent of the pure P3HT film in Fig. 8(c), but in this case the fibers are much thicker.

Unlike the pristine P3HT films in Fig. 8, which were spin-coated onto silicon substrates, the colloid films in Fig. 9 were drop cast onto glass. Thus, apart from differences in solvent (water versus CF:DCM) and the nature of the colloidal particles, the disparities in particle-particle and particle-substrate interactions, wetting, and drying time, etc. all contribute to the assembly of the films. However, unlike the P3HT films in Fig. 8, which are cast from different solvent mixtures, the colloid films in Fig. 9 share the same aqueous SDS medium. Thus, the variations in the film morphology are largely dependent on the characteristics of the colloidal particles, and, by extension, the aggregate dispersions used to prepare the aqueous colloid. These findings are significant because they show that the varying characteristics of the aggregate dispersions can be exploited to not only tune the properties of the aqueous colloids, but also the films processed from the colloids.

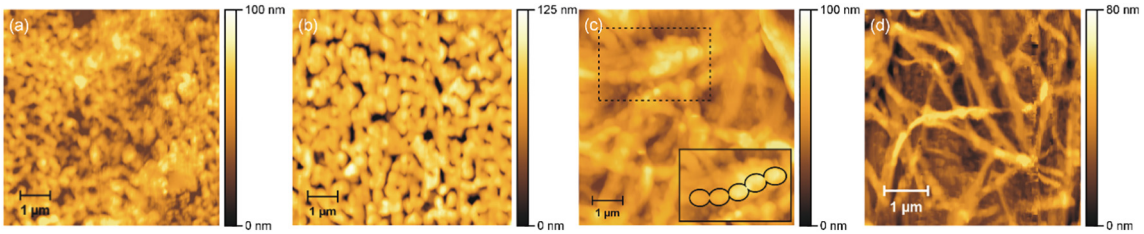

Fig. 9. Tapping mode AFM (TT-AFM) height images of P3HT films ($M_n \approx 30$ kDa) drop cast from SDS-stabilized colloids prepared using the mini-emulsion and 1 mg·mL^{-1} aggregate dispersions in (a) 80:20, (b) 60:40, (c) 40:60, and (d) 20:80 CF:DCM mixtures. The inset in (c) emphasizes the linear arrangement of the spheroidal structures in the region of film highlighted in the upper left of the image.

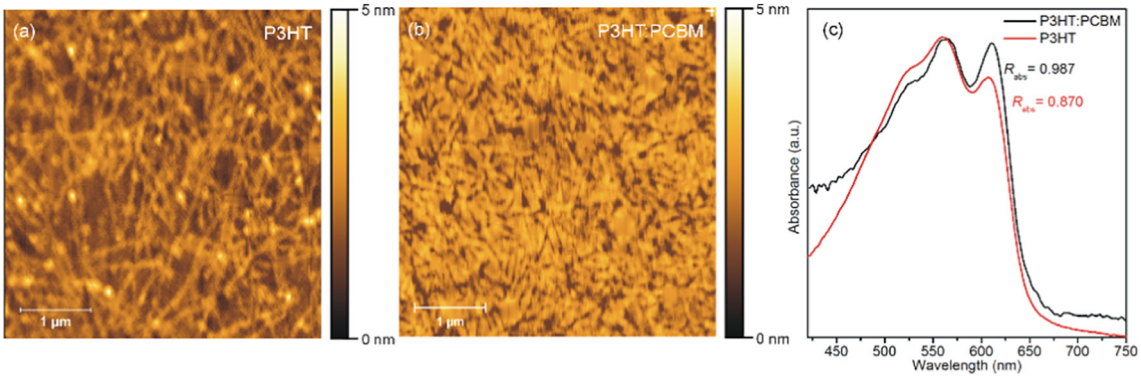

Fig. 10. Atomic force microscopy (AFM) height images of (a) P3HT and (b) P3HT:PCBM films on silicon substrates spun-cast (1000 rpm) from aggregate dispersions fabricated in 60:40 CF:DCM solvent mixtures. (c) Comparison of the UV/Vis spectra and vibronic structure (R_{abs}) of the P3HT and P3HT:PCBM films in shown in (a) and (b). The films in (c) were processed by spin coating (1000 rpm) the dispersions onto glass substrates.

Although a detailed discussion is beyond the scope of this study, it is interesting to briefly mention that the P3HT:PCBM dispersions have a notable impact on the morphology of the spin-coated films. Fig. 10 (a) and (b) are exemplary films processed using, respectively, P3HT and P3HT:PCBM dispersions in 60:40 CF:DCM. The P3HT dispersion produces a film composed of long, high aspect ratio fibers, whereas the P3HT:PCBM film is a dense network of shorter, low aspect ratio structures. Additionally, as shown in Fig. 10(c), the UV/Vis spectra of the films reveals that compared to the pure P3HT film, the P3HT:PCBM film maintains a high intrachain order, $R_{abs} \approx 0.987$, relative to the liquid phase dispersion, $R_{abs} \approx 1.024$. The characteristics of the of the P3HT:PCBM dispersions that more readily preserve the intrachain order during the assembly of the film, may, in turn, play a similar role in promoting the high intrachain order observed in the colloids. A more detailed investigation of this topic is currently underway.

4. Conclusions

SDS-stabilized colloids of pristine P3HT processed from amorphous P3HT/CF solutions exhibit large intrachain structural disorder, which can have a detrimental impact on their performance in functional materials and composites. Solvent mixtures of chloroform (CF) and dichloromethane (DCM) can be used to fabricate aggregate dispersions with tunable extent of aggregation and intrachain order, and these aggregate pre-cursors yield aqueous colloids with improved intrachain order. The results of this study reveal a strong correlation between the intrachain order of the aggregate dispersion and colloids, thereby indicating that the structural characteristics of the aggregates are effectively transferred to the colloids. Based on the anomalously high molecular order in colloids processed from dispersions with relatively low extent of aggregation, we contend that the identity of the organic solvents and the composition of the mixtures used to fabricate the dispersions are critical to the assembly of P3HT in the colloids. Furthermore, when P3HT aggregation in CF:DCM mixtures is performed in the presence of PCBM, the intrachain order in the resulting SDS-stabilized P3HT:PCBM colloids is significantly higher than the corresponding colloids of pure P3HT. Although this trend was corroborated with a different P3HT sample, the origin of this behavior is still unknown at this time. Finally, using atomic force microscopy notable changes were observed in the dominant structural motifs and morphology of films processed from the set of aqueous colloids of P3HT, but not in a way that readily relates to films processed from the aggregate dispersions of pure P3HT. Thus, in contrast to solutions of amorphous P3HT and P3HT:PCBM, the aggregate dispersions can be utilized to modify the characteristics of the aqueous colloids, as well as the films. Additional work using different solvent mixtures, P3HT and PCBM concentrations, and investigating the time dependence of the colloid formation is currently underway to reveal more details about the fundamental behavior of the systems.

Acknowledgement

The authors acknowledge the donors of the American Chemical Society Petroleum Research Fund (55397-UR7) for support of this research.

Appendix A. Supplementary data

Supplementary data to this article can be found online at https://doi.org/10.1016/j.molliq.2019.01.031.

References

[1] C. Müller, M. Aghamohammadi, S. Himmelberger, P. Sonar, M. Garriga, A. Salleo, M. Campoy-Quiles, One-step macroscopic alignment of conjugated polymer systems by epitaxial crystallization during spin-coating, Adv. Funct. Mater. 23 (2013) 2368–2377.
[2] Y. Gao, T.P. Martin, E.T. Niles, A.J. Wise, A.K. Thomas, J.K. Grey, Understanding morphology-dependent polymer aggregation properties and photocurrent generation in polythiophene/fullerene solar cells of variable compositions, J. Phys. Chem. C 114 (2010) 15121–15128.
[3] Y. Yuan, J. Shu, P. Liu, Y. Zhang, Y. Duan, J. Zhang, Study on π–π interaction in H- and J-aggregates of poly(3-hexylthiophene) nanowires by multiple techniques, J. Phys. Chem. B 119 (2015) 8446–8456.
[4] A. Tamanai, S. Beck, A. Pucci, Mid-infrared characterization of thiophene-based thin polymer films, Displays 34 (2013) 399–405.
[5] C.-P. Chen, S.-H. Chan, T.-C. Chao, C. Ting, B.-T. Ko, Low-bandgap poly(thiophene-phenylene-thiophene) derivatives with broaden absorption spectra for use in high-performance bulk-heterojunction polymer solar cells, J. Am. Chem. Soc. 130 (2008) 12828–12833.
[6] J.-H. Kim, J.H. Hwang, J. Suh, S. Tongay, S. Kwon, C.C. Hwang, J. Wu, J. Young Park, Work function engineering of single layer graphene by irradiation-induced defects, Appl. Phys. Lett. 103 (2013), 171604. .
[7] C.M. Hansen, The three dimensional solubility parameter- a key to paint component affinities I, J. Paint Technol. 39 (1967) 104–117.
[8] C.M. Hansen, The three dimensional solubility parameter - a key to paint component affinities II, J. Paint Technol. 39 (1967) 505–510.
[9] J. Yu, Y. Zheng, J. Huang, Towards high performance organic photovoltaic cells: a review of recent development in organic photovoltaics, Polymers 6 (2014) 2473–2509.
[10] M. Chang, G. Lim, B. Park, E. Reichmanis, Control of molecular ordering, alignment, and charge transport in solution-processed conjugated polymer thin films, Polymers 9 (2017) 212.
[11] M. Brinkmann, Structure and morphology control in thin films of regioregular poly (3-hexylthiophene), J. Polym. Sci. Polym. Phys. 49 (2011) 1218–1233.
[12] W. Oosterbaan, V. Vrindts, S. Berson, S. Guillerez, O. Douheret, B. Ruttens, J. D'Haen, P. Adriaensens, J. Manca, L. Lutsen, D. Vanderzande, Efficient formation, isolation and characterization of poly(3-alkylthiophene) nanofibres: probing order as a function of side-chain length, J. Mater. Chem. 19 (2009) 5424–5435.
[13] J.D. Roehling, I. Arslan, A.J. Moule, Controlling microstructure in poly(3-hexylthiophene) nanofibers, J. Mater. Chem. 22 (2012) 2498–2506.
[14] T.P. Martin, A.J. Wise, E. Busby, J. Gao, J.D. Roehling, M.J. Ford, D.S. Larsen, A.J. Moulé, J.K. Grey, Packing dependent electronic coupling in single poly(3-hexylthiophene) H- and J-aggregate nanofibers, J. Phys. Chem. B 117 (2012) 4478–4487.
[15] E.T. Niles, J.D. Roehling, H. Yamagata, A.J. Wise, F.C. Spano, A.J. Moulé, J.K. Grey, J-aggregate behavior in poly-3-hexylthiophene nanofibers, J. Phys. Chem. Lett. 3 (2012) 259–263.
[16] M. Baghgar, J. Labastide, F. Bokel, I. Dujovne, A. McKenna, A.M. Barnes, E. Pentzer, T. Emrick, R. Hayward, M.D. Barnes, Probing inter- and intrachain exciton coupling in

isolated poly(3-hexylthiophene) nanofibers: effect of solvation and regioregularity, J. Phys. Chem. Lett. 3 (2012) 1674–1679.
[17] C. Scharsich, R.H. Lohwasser, M. Sommer, U. Asawapirom, U. Scherf, M. Thelakkat, D. Neher, A. Köhler, Control of aggregate formation in poly(3-hexylthiophene) by solvent, molecular weight, and synthetic method, J. Polym. Sci. Polym. Phys. 50 (2012) 442–453.
[18] K. Zhao, L. Xue, J. Liu, X. Gao, S. Wu, Y. Han, Y. Geng, A new method to improve poly (3-hexyl thiophene) (P3HT) crystalline behavior: decreasing chains entanglement to promote order−disorder transformation in solution, Langmuir 26 (2010) 471–477.
[19] R. Potai, A. Kamphan, R. Traiphol, Conformational change, intrachain aggregation and photophysical properties of regioregular poly(3-octylthiophene) in alkanes, J. Polym. Sci. Polym. Phys. 51 (2013) 1288–1297.
[20] K.J. Ihn, J. Moulton, P. Smith, Whiskers of poly(3-alkylthiophene)s, J. Polym. Sci. Polym. Phys. 31 (1993) 735–742.
[21] J.E. Millstone, D.F.J. Kavulak, C.H. Woo, T.W. Holcombe, E.J. Westling, A.L. Briseno, M.F. Toney, J.M.J. Fréchet, Synthesis, properties, and electronic applications of size-controlled poly(3-hexylthiophene) nanoparticles, Langmuir 26 (2010) 13056–13061.
[22] D.S. Boucher, Effects of evaporation velocity and film thickness on poly(3-hexylthiophene) thin films processed from aggregate dispersions in binary solvent mixtures, J. Polym. Sci. Polym. Phys. 55 (2017) 330–343.
[23] M.P. Gordon, L.T. Lloyd, D.S. Boucher, Poly(3-hexylthiophene) films prepared using binary solvent mixtures, J. Polym. Sci. Polym. Phys. 54 (2016) 624–638.
[24] C.E. Johnson, D.S. Boucher, Poly(3-hexylthiophene) aggregate formation in binary solvent mixtures: an excitonic coupling analysis, J. Polym. Sci. Polym. Phys. 52 (2014) 526–538.
[25] C.E. Johnson, M.P. Gordon, D.S. Boucher, Rationalizing the self-assembly of poly-(3-hexylthiophene) using solubility and solvatochromic parameters, J. Polym. Sci. Polym. Phys. 53 (2015) 841–850.
[26] S. Marni, B. David, Poly(3-hexylthiophene) aggregation at solvent–solvent interfaces, J. Polym. Sci. Polym. Phys. 56 (2018) 999–1011.
[27] M. Sapolsky, J. McFaddin, D. Boucher, Aggregation behavior of poly(3-hexylthiophene) in solvent mixtures: linear solvation energy relationship (LSER) modeling and COSMO-RS calculations, Macromol. Chem. Phys. 219 (2018), 1700545. .
[28] J. Pecher, S. Mecking, Nanoparticles of conjugated polymers, Chem. Rev. 110 (2010) 6260–6279.
[29] K. Landfester, Miniemulsion polymerization and the structure of polymer and hybrid nanoparticles, Angew. Chem. Int. Ed. 48 (2009) 4488–4507.
[30] B. Tan, H. Pan, B.M. Budhlall, M.J. Sobkowicz, Poly(3-hexylthiophene)/poly(styrene) blended colloids: exploiting the effects of composition and marginal solvent, Colloids Surf. A Physicochem. Eng. Asp. 539 (2018) 221–228.
[31] B. Tan, Y. Li, M.F. Palacios, J. Therrien, M.J. Sobkowicz, Effect of surfactant conjugation on structure and properties of poly(3-hexylthiophene) colloids and field effect transistors, Colloids Surf. A Physicochem. Eng. Asp. 488 (2016) 7–14.
[32] J.J. Richards, K.M. Weigandt, D.C. Pozzo, Aqueous dispersions of colloidal poly(3-hexylthiophene) gel particles with high internal porosity, J. Colloid Interface Sci. 364 (2011) 341–350.
[33] A. Jouyban, S. Soltanpour, Prediction of dielectric constants of binary solvents at various temperatures, J. Chem. Eng. Data 55 (2010) 2951–2963.
[34] J.T. Lopez Navarrete, G. Zerbi, Lattice dynamics and vibrational spectra of polythiophene. I. Oligomers and polymer, J. Chem. Phys. 94 (1991) 957–964.
[35] J.T. Lopez Navarrete, G. Zerbi, Lattice dynamics and vibrational spectra of polythiophene. II. Effective coordinate theory, doping induced, and photoexcited spectra, J. Chem. Phys. 94 (1991) 965–970.
[36] B.A. Gregg, Excitonic solar cells, J. Phys. Chem. B 107 (2003) 4688–4698.
[37] H. Hoppe, N.S. Sariciftci, Organic solar cells: an overview, J. Mater. Res. 19 (2004) 1924–1945.
[38] B.C. Thompson, J.M.J. Frechet, Polymer-fullerene composite solar cells, Angew. Chem. Int. Ed. 47 (2008) 58–77.
[39] A.J. Moulé, K. Meerholz, Controlling morphology in polymer–fullerene mixtures, Adv. Mater. 20 (2008) 240–245.
[40] S. Cataldo, B. Pignataro, Polymeric thin films for organic electronics: properties and adaptive structures, materials, (Basel) Switz. 6 (2013) 1159–1190.
[41] J. Yu, Y. Zheng, J. Huang, Towards high performance organic photovoltaic cells: a review of recent development in organic photovoltaics, Polymers 6 (2014).
[42] S.-S. Sun, N.S. Saraciftci, Organic Photovoltaics: Mechanisms, Materials, and Devices, CRC Press, Boca Raton, 2005.